

DOI: 10.13476/j.cnki.nsbdtk.2021.0082

张梦中,潘坚文,王进廷,等.小湾拱坝运行期温度场反演与应力仿真分析[J].南水北调与水利科技(中英文),2021,19(4):786-794,813. ZHANG M Z, PAN J W, WANG J T, et al. Feedback analysis on temperature field and stress simulation of Xiaowan arch dam in the operation period[J]. South-to-North Water Transfers and Water Science & Technology, 2021, 19(4): 786-794, 813. (in Chinese)

小湾拱坝运行期温度场反演与应力仿真分析

张梦中¹, 潘坚文¹, 王进廷¹, 迟福东²

(1. 清华大学水沙科学与水利水电工程国家重点实验室, 北京 100084; 2. 华能澜沧江水电股份有限公司, 昆明 650214)

摘要:拱坝所处的运行环境复杂, 受力状态复杂, 其真实的工作状态往往与其设计状态存在一定的差异, 因此开展基于坝体温度和变形监测资料, 反演坝体与基岩材料参数, 仿真坝体的应力状态的研究。通过有限元方法, 基于小湾拱坝实测温度, 拟合上下游坝面的温度边界条件, 并对拱坝运行期温度场进行了仿真; 基于变形监测资料, 反演坝体和基岩弹性模量; 基于反演得到的坝体温度场与材料弹性模量, 对小湾拱坝进行应力仿真分析。研究表明: 小湾拱坝下游面温度分布总体呈现出两侧坝段高于中间坝段的规律; 运行期坝体混凝土的弹性模量相对于试验值约提高 30%; 在冬季时, 上游坝面水位以上部分出现局部拉应力, 下游坝面在坝基交界面附近由于应力集中出现局部拉应力, 但不至于影响工程安全运行。

关键词:小湾拱坝; 温度场; 材料参数; 反演分析; 应力仿真

中图分类号: TV31 文献标志码: A 开放科学(资源服务)标志码(OSID):



温度荷载是混凝土高拱坝在运行期间所承受的主要荷载之一。拱坝温度荷载的计算方法是根据运行期坝体混凝土温度与封拱温度之间的差值确定的。一般而言, 拱坝的封拱温度场容易获得, 而由于受到气候条件、结构形式与运行方式等的影响, 拱坝运行期坝体温度场的分析较为复杂, 其难点主要在于确定拱坝运行期间的温度边界条件。拱坝运行期间的温度边界, 主要由坝面与库水接触边界、坝面与空气接触边界这两部分构成。与库水接触的坝面温度可认为等于库水温度, 人们通常使用朱伯芳院士^[1]提出的库水温度估算公式进行计算, 这种方法计算简单, 但是对 300 m 级高坝的库水温度的分析有一定的偏差^[2]。因此, 有学者^[3-4]提出使用数值模型来分析库水温度, 但是这类方法需要已知来流温度、出流温度等参数, 在实际工程中的应用受到限制。与空气接触的坝面受到太阳辐射作用、对流换

热的影响, 坝面温度的分布更为复杂。因此, 王进廷等^[5]根据实测温度拟合坝面温度分布函数, 得到二滩拱坝运行期下游坝面的温度分布边界条件; Jin 等^[6]采用 ASHRAE 晴空模型分析二滩拱坝下游坝面温度分布, 该模型表现出一定的适用性。

此外, 由于拱坝是空间三维壳体结构, 在运行期间受力状态复杂, 坝体混凝土及其基岩的弹性模量常常与设计值或试验值有所不同^[7]。为准确评估拱坝在运行期间的结构性态, 有必要对坝体及其基岩的弹性模量进行反演分析。拱坝运行期坝体混凝土及其基岩弹性模量的反演分析, 通常是已知坝体运行期间的实测位移资料来反推坝体与基岩的弹性模量。总的来说, 可以将坝体及其基岩弹性模量反演方法归结为两大类: 第一类是传统的优化方法, 如单纯形法^[8]、高斯-牛顿法^[9]、Levenberg-Marquardt 算法^[10]等; 第二类是随着计算机技术的发展、并行运

收稿日期: 2020-12-31 修回日期: 2021-05-06 网络出版时间: 2021-05-12

网络出版地址: <https://kns.cnki.net/kcms/detail/13.1430.tv.20210511.1953.002.html>

基金项目: 国家自然科学基金(52022047; 51725901; 51639006); 华能科技项目(HNKJ18-H25)

作者简介: 张梦中(1998—), 男, 河南周口人, 主要从事高坝健康监测研究。E-mail: zzm20@mails.tsinghua.edu.cn

通信作者: 王进廷(1973—), 男, 山西吕梁人, 教授, 博士, 主要从事高坝健康监测研究。E-mail: wangjt@tsinghua.edu.cn

算能力的提高而出现的智能反演方法,如粒子群算法^[11-13]、神经网络算法^[14-16]、遗传算法^[17-20]等。

作为 300 m 级的高拱坝,小湾拱坝运行期真实工作性态的研究具有重要的意义,但目前对小湾拱坝温度场的研究多限于施工期间以及单个坝段,针对小湾拱坝运行期间全坝段的温度场、应力场的分析还有待深入。因此,基于小湾拱坝原型观测坝体温度,拟合上下游坝面温度分布规律作为坝面的温度边界条件,反演得到小湾拱坝运行期全坝段的瞬态温度场,并以小湾拱坝的垂线观测资料作为比较对象,反演得出坝体及其基岩的弹性模量,据此对小湾拱坝在水压、自重与温度荷载作用下的应力进行仿真分析,揭示大坝运行期的应力状态。

1 计算方法

1.1 温度场有限元计算

设有一个均匀的、各向同性的混凝土固体,不考虑混凝土的绝热升温,其热传导方程^[1]为

$$\frac{\partial T}{\partial \tau} = a \left(\frac{\partial^2 T}{\partial x^2} + \frac{\partial^2 T}{\partial y^2} + \frac{\partial^2 T}{\partial z^2} \right) + \frac{Q}{c\rho} \quad (1)$$

式中: T 为温度,℃; a 为导热系数, m^2/h ; x 、 y 、 z 为直角坐标; τ 为时间; c 为比热容, $\text{kJ}/(\text{kg} \cdot \text{K})$; ρ 为密度 kg/m^3 ; Q 为单位体积的混凝土立方体由于水泥水化热的作用,在单位时间内所产生的热量, $\text{kJ}/(\text{m}^3 \cdot \text{h})$ 。

稳定温度场有 $\frac{\partial T}{\partial \tau} = 0$,计算域内的求解方程^[21]

可以表示为

$$\mathbf{K}\boldsymbol{\phi} = \mathbf{P} \quad (2)$$

式中: \mathbf{K} 是热传导矩阵; $\boldsymbol{\phi} = [\phi_1 \phi_2 \phi_3 \cdots \phi_n]$ 是结点温度列阵; \mathbf{P} 是温度荷载列阵。

计算瞬态温度场的矩阵方程可以表示为

$$\mathbf{C}\dot{\boldsymbol{\phi}} + \mathbf{K}\boldsymbol{\phi} = \mathbf{P} \quad (3)$$

式中: \mathbf{C} 表示热容矩阵; $\dot{\boldsymbol{\phi}} = \text{d}\boldsymbol{\phi}/\text{d}t$,表示结点温度对时间的导数列阵; \mathbf{K} 为热传导矩阵; \mathbf{P} 为温度荷载列阵。

1.2 温度场边界条件

温度场边界条件可由以下 3 种方式给出^[1]。

第一类边界条件。混凝土表面温度为已知函数 $T(\tau) = f(\tau)$ (4)

第二类边界条件。混凝土表面的热流量是时间的已知函数

$$-\lambda \frac{\partial T}{\partial n} = f(\tau) \quad (5)$$

第三类边界条件。固体与流体接触的情况,在

接触面会产生对流换热

$$-\lambda \frac{\partial T}{\partial n} = \beta(T - T_a) \quad (6)$$

式(4)~(6)中: λ 为导热系数, $\text{kJ}/(\text{m} \cdot \text{h} \cdot \text{K})$; β 为表面放热系数, $\text{kJ}/(\text{m}^2 \cdot \text{h} \cdot \text{K})$; T_a 为气温,℃。

1.3 拱坝反演分析方法

拱坝坝体与基岩材料的反演分析,是根据实测的坝体对环境量(温度、水位等)的响应,确定工程计算与分析所需的物理力学参数的一种方法。实质上,可以将材料弹性模量的反演问题理解为一个寻优过程,其目标函数是实测位移与数值计算位移差值的平方和^[22]

$$F(\mathbf{X}) = \sum_{i=1}^n [u_i(\mathbf{X}) - u_i^*(\mathbf{X})]^2 \rightarrow \min \quad (7)$$

式中: \mathbf{X} 是物理力学参数向量; n 为测点个数; u_i 是第 i 个测点数值计算位移; u_i^* 是第 i 个测点实测位移。

由于数值计算位移是使用有限元方法得到的,所以以上的目标函数应满足的约束条件为

$$[\mathbf{k}]\{\mathbf{u}\} = \{\mathbf{R}\} \quad (8)$$

式中: $[\mathbf{k}]$ 为结构整体刚度矩阵; $\{\mathbf{u}\}$ 为节点位移向量; $\{\mathbf{R}\}$ 为节点等效荷载向量。

2 小湾拱坝监测仪器布置情况

小湾拱坝最大坝高 294.5 m,正常蓄水位为 1 240 m。工程设置各类监测项目,包括温度、变形和应力等。

2.1 温度监测

在 15、22 和 29 号坝段上游面安放铜电阻温度计,监测水库水温。在 9、15、22、29 和 35 号坝段下游面埋设温度计,监测下游坝面温度。在 9、15、22、29 和 35 号坝段坝体内部埋设温度计,监测大坝的温度场。由于各测点温度测值在不同年份内变化规律基本一致,故本文采用 2016 年温度测值进行分析。

2.2 变形监测

在 4、9、15、22、29、35 和 41 号坝段的各层廊道中分段设置正垂线^[23],监测坝体的水平变形和挠度,见图 1。其中 4 号与 41 号坝段垂线自投入使用以来,受环境干扰及仪器本身精确度等因素的影响,监测数据质量差,后续反演计算中不使用这些测点。

垂线监测系统的原始监测数据需要经过修正后才能使用,一般是根据监测数据变化规律去除异常值。图 2 为测点 A25-PL-01 原始监测资料与修正后的数据。

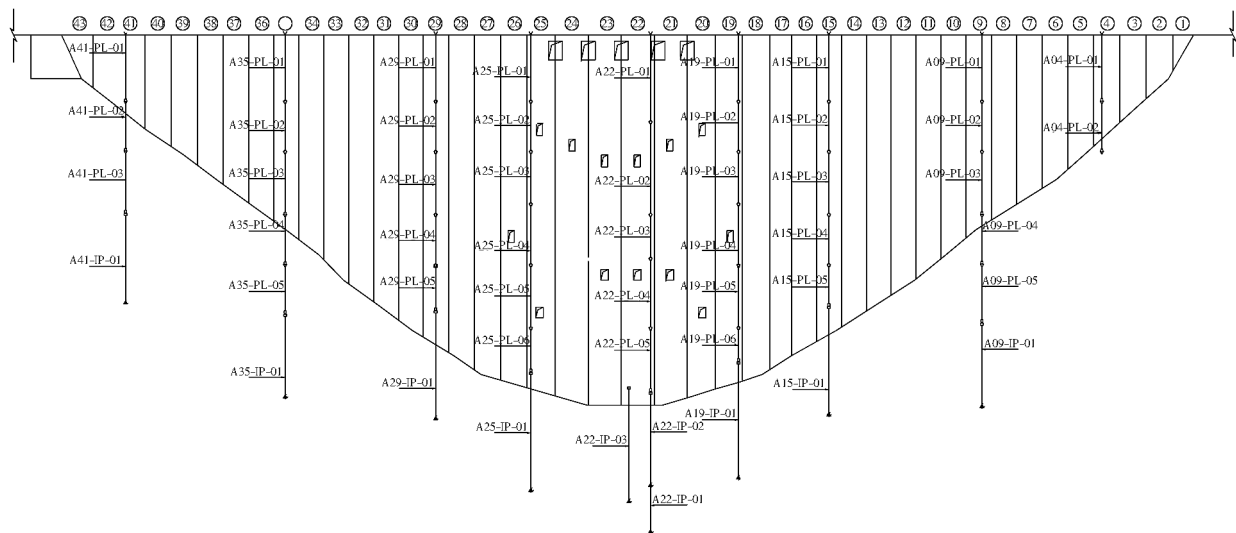


图 1 小湾拱坝垂线系统布置

Fig. 1 Layout of plumb lines for Xiaowan arch dam

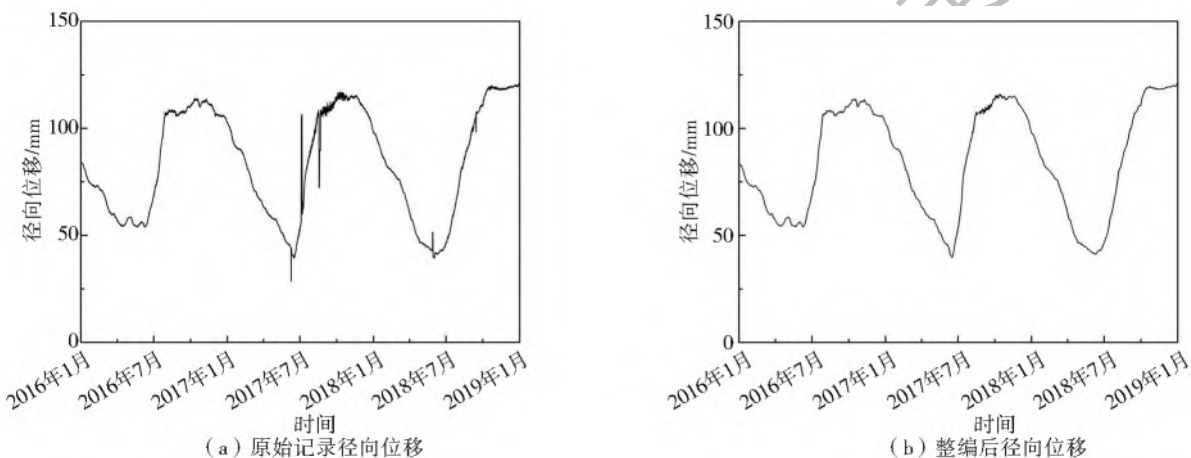


图 2 垂线测点 A25-PL-01 径向位移测值

Fig. 2 Displacements monitored by plumb line A25-PL-01

3 计算模型

考虑到原始观测资料的完备性,计算中采用 2016 年监测数据。有限元中计算步长的选取十分重要,本研究以旬为计算步长,这样既可以保证反演分析的精度,又不至于产生过大的计算量,相应的荷载与边界条件也按旬为单位进行选取。

3.1 有限元模型

图 3 为小湾拱坝-基岩系统的有限元模型,模型范围为:上游至 F₇ 断层,下游边界延伸 780 m,左右岸与向下均延伸一倍坝高,坝顶高程为 1 245 m,截断地基底边界高程为 645 m。整个模型共包含 435 666 个节点、411 094 个单元,其中坝体部分包含 55 790 个单元。

3.2 材料参数试验值

坝体混凝土共分为 A、B、C 等 3 个分区,各分区混凝土物理力学参数试验值见表 1。

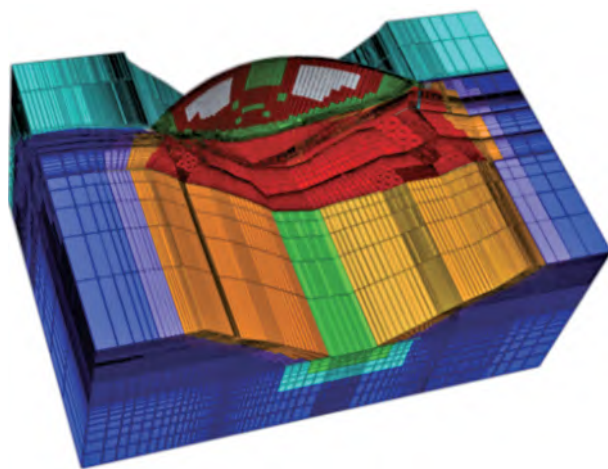


图 3 小湾拱坝有限元模型

Fig. 3 Finite element model of Xiaowan arch dam

地基岩体主要分为 6 种,力学性质见表 2。此外,模型中精确模拟了坝址处的断层与蚀变带情况。对于建基面下的卸荷岩体,为简化分析模型,对卸荷带、过渡带和基本正常带进行概化处理,分高程、卸

荷深度与上下游位置不同进行分组,共分为 180 组材料,变形模量试验值为 7~24 GPa。

表 1 混凝土与基岩热力学参数

Tab. 1 Thermodynamic parameters of dam concrete and foundation rock

材料/分区	密度/ ($\text{Kg}\cdot\text{m}^{-3}$)	比热容/ [$\text{KJ}\cdot(\text{Kg}\cdot\text{K}^{-1})$]	导热系数/ [$\text{KJ}\cdot(\text{m}\cdot\text{h}\cdot\text{K})^{-1}$]	弹性模量/ GPa
A 区	2 500	1.047	8.479	32.1
B 区	2 500	1.056	8.227	31.1
C 区	2 500	1.072	8.016	30.1
基岩	2 755	1.072	8.016	

表 2 主要基岩物理力学参数

Tab. 2 Mechanical parameters of main foundation rock

岩体类别	μ	E_0/GPa	f'	c'/MPa
I 类	0.22	25	1.5	2.2
II a 类	0.26	22	1.5	2.0
II b 类	0.27	20	1.4	1.8
II c 类	0.27	20	1.4	1.8
II d 类	0.28	18	1.4	1.6
III 类	0.28	6	1.2	1.2

3.3 温度场计算边界条件

拱坝温度场计算的边界条件主要包含以下几个方面^[1,6]:

水位以下坝面,实质上是第三类边界条件,但由于库水与混凝土表面放热系数很大,所以可以将其等效为第一类边界条件,相应温度为实测水温。

水位以上坝面,为混凝土与空气接触的边界条件,实质上是第三类边界条件。根据坝面温度计实

测值,拟合上下游坝面温度分布函数将其转化为第一类边界条件。

河谷、河岸在水位以下部分,按照第一类边界条件处理,取值为相应高程实测水温。河谷、河岸在水位以上部分,将其转化为第一类边界条件,具体取值为每旬平均气温。

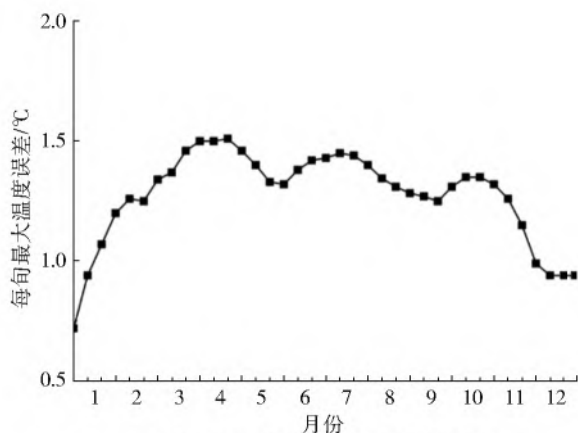
地基深部温度主要受地温影响,监测成果表明小湾拱坝坝基温度总体趋于稳定,可认为地基地面为第一类边界条件。地基侧面按绝热边界处理。

3.4 坝面温度分布拟合方案

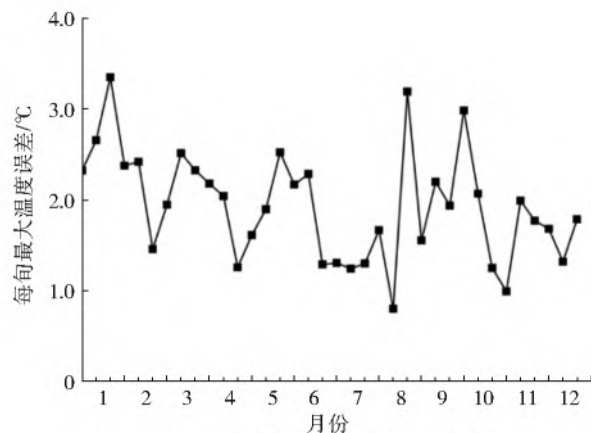
水位以下的坝面与库水接触,温度受库水影响较大,而水温一般可以假定为在高程方向上成层分布,故认为水位以下坝面温度只是高程 z 的函数^[5]。

下游坝面水位以上部分,坝面温度分布不仅与高程 z 相关,也与空间 x 坐标相关,故采用 $T=a+bx+cz+dxz+(mx^2)+(nz^2)$ 进行拟合。为避免引入平方项而造成两侧坝肩处出现异常温度值的问题,假定 1~9 号坝段下游坝面温度分布规律与 9 号横缝处温度分布规律相同,35~43 号坝段温度分布规律与 35 号横缝处温度分布规律相同。其中, a, b, c, d, m, n 是待反演的多项式系数。

图 4 为小湾拱坝坝面温度计实测温度与拟合结果的误差情况。上游坝面测点温度误差基本在 $1.0\text{ }^\circ\text{C}$ 以内;下游坝面测点温度误差基本在 $2.5\text{ }^\circ\text{C}$ 以内。这表明坝面温度拟合结果可以反映坝面实际温度分布规律。个别测点误差较大的原因为:位于泄洪表孔附近、靠近坝底的温度测点,由于受泄水或地温的影响,温度测值不符合坝面温度分布规律。



(a) 上游坝面测点每旬最大温度误差



(b) 下游坝面测点每旬最大温度误差

图 4 坝面温度拟合误差情况

Fig. 4 Fitting errors between measured temperatures and calculated temperatures on dam surface

3.5 材料参数反演计算工况

材料参数反演过程中,荷载考虑静水压力、自重荷载和温度荷载。其中静水压力根据上下游每旬平

均水位进行计算。温度荷载根据反演得到的运行期温度场与封拱温度场之间的差值进行确定。表 3 为小湾拱坝各灌区的封拱温度。

表 3 小湾拱坝设计封拱温度

Tab. 3 The joint closure temperature field of Xiaowan arch dam

单位: °C

封拱温度 分区	950.5 ≤ z ≤ 989.0	989.0 < z ≤ 1 037.0	1 037.0 < z ≤ 1 071.5	1 071.5 < z ≤ 1 107.0	1 107.0 < z ≤ 1 184.5	1 184.5 < z ≤ 1 245.0
上游区	12	12	12			
中游区	14	14	14	14	15	16
下游区	16	17	18			

注: z 为高程, 单位为 m。

3.6 材料参数反演过程

小湾拱坝一地基系统材料分区较多, 材料参数反演分析是一项复杂的工作, 为减少反演工作量, 选取各种材料弹性模量的试验值作为材料参数反演分析的初始计算工况。反演分析过程中, 以各测点高水位与低水位之间的相对位移作为调整依据, 调整各分区材料弹性模量直至计算位移与实测位移变化规律一致、数值误差较小。

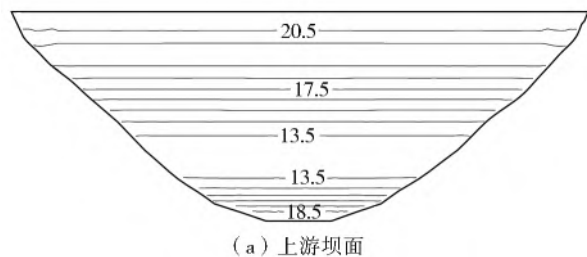
4 计算结果

4.1 温度场反演结果

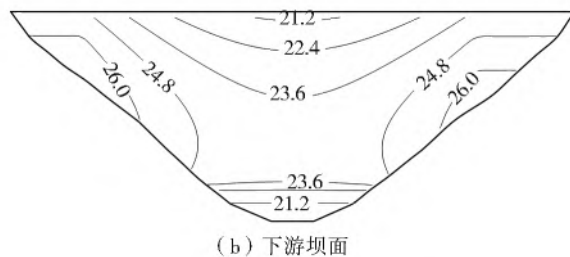
按照上述计算模型与温度边界, 反演计算得到小湾拱坝 2016 年各旬瞬态温度场。选取 54 支坝内温度计分析坝内实测温度与反演计算温度之间的误

差情况, 结果表明, 反演计算温度与实测值每旬均方根误差为 1.26~1.40 °C, 其中 37 支温度测点的误差控制在 1 °C 以内, 这表明反演计算结果可以反映小湾拱坝坝内实际温度场。个别测点误差较大的原因是安装在闸墩、孔口与廊道附近的仪器受到孔口泄水及混凝土表面散热影响较大, 而有限元模型中并没有包含这些附属结构。

图 5~7 为小湾拱坝 2016 年 4 月上旬和 10 月上旬温度分布, 从图中可以看出: 上游坝面温度主要受库水的影响, 水位以下部分温度变化不大; 上游坝面在靠近坝底部分, 由于受到地温及坝前堆渣的影响, 坝面温度会略有升高, 为 17~19 °C; 下游坝面温度受气温影响较大, 总体呈现出两侧坝段温度较高, 中间坝段温度较低的趋势。



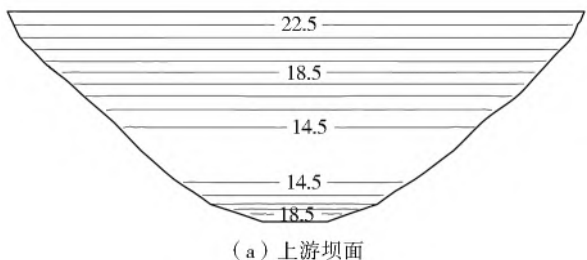
(a) 上游坝面



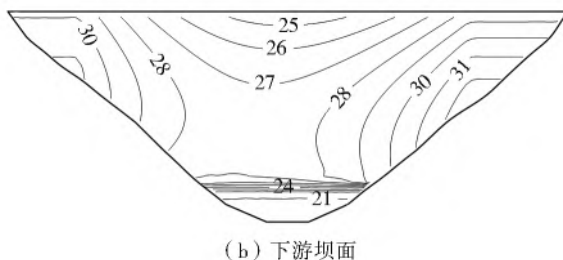
(b) 下游坝面

图 5 2016 年 4 月上旬坝面温度分布(单位: °C)

Fig. 5 Dam surface temperature distribution in early April 2016(Unit: °C)



(a) 上游坝面



(b) 下游坝面

图 6 2016 年 10 月上旬坝面温度分布(单位: °C)

Fig. 6 Dam surface temperature distribution in early October 2016(Unit: °C)

4.2 材料参数反演结果

反演得到材料弹性模量取值见表 4, 其中, C_R 表示右岸坝段 C 区混凝土, C_L 表示左岸坝段 C 区混凝土, I_R 表示右岸地基中的 I 类岩体, I_L 表示左岸地基中的 I 类岩体; 此外, 右岸卸荷岩体、左岸卸荷岩体与坝址区断层变形模量反演值相对于试验值分

别提高 1.20 倍、1.45 倍与 1.20 倍。由反演结果可知: 坝体混凝土各分区弹性模量相对于试验值提高约 30%; 坝址处基岩变形模量比试验值提高 20%~45%。

根据反演得到的弹性模量, 计算出小湾拱坝 2016—2018 年位移情况并与实测位移进行对比(图

8),其中,径向位移以向下游为正,以2016年1月上旬为径向位移的“零点”,可以看出:计算位移与实测位移变化规律一致、误差较小;目前时效作用还未完全收敛,坝体总体存在着向下游缓慢变形的趋势。

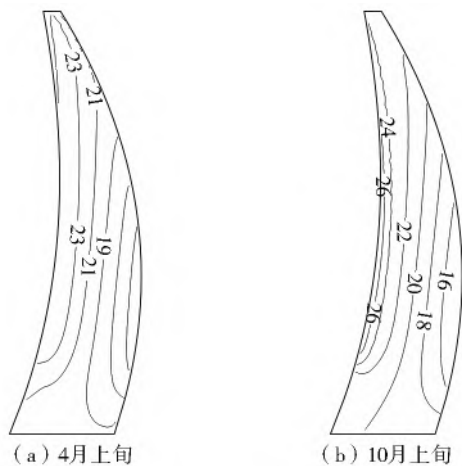
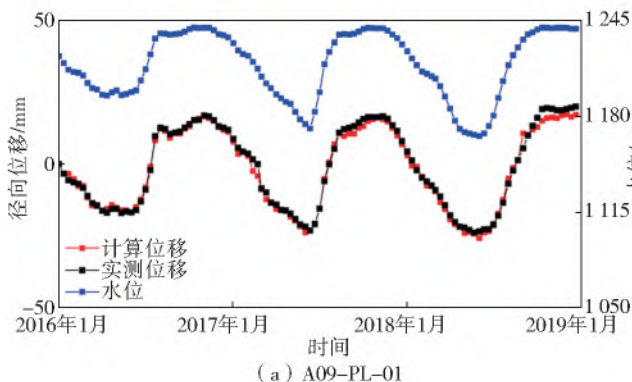
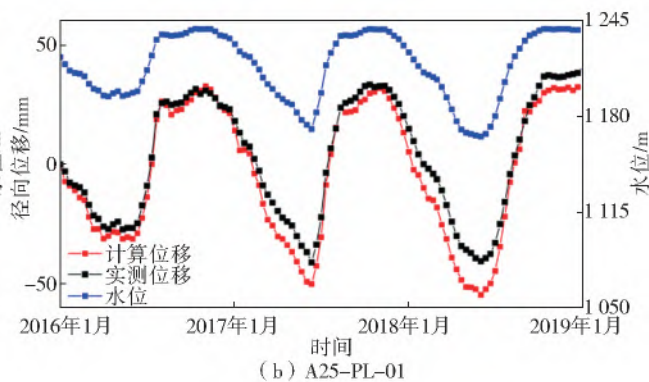


图7 2016年拱冠梁断面温度分布(单位:℃)

Fig. 7 Temperature distribution of crown beam section in 2016(Unit:℃)

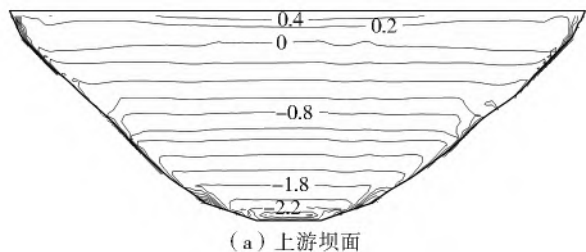


(a) A09-PL-01

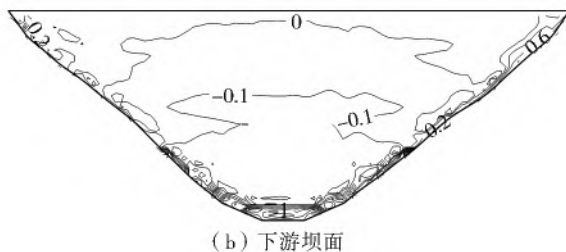


(b) A25-PL-01

图8 坝顶测点径向位移实测值与计算值对比
Fig. 8 Comparisons of computed radial displacements with the measured values of dam crest



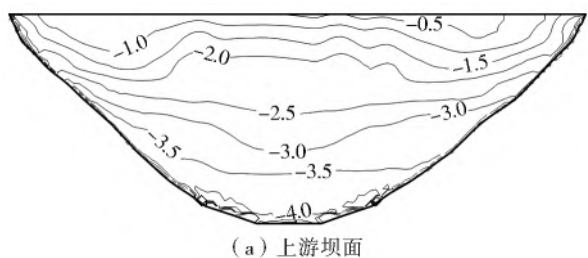
(a) 上游坝面



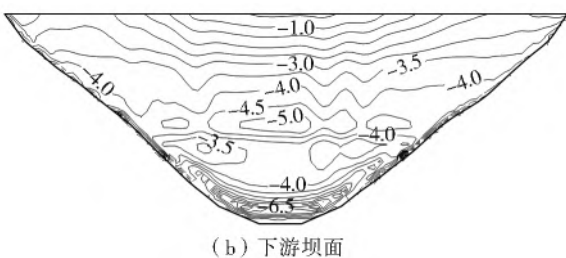
(b) 下游坝面

图9 4月上旬坝面最大主应力分布(单位:MPa)

Fig. 9 Maximum principal stress distribution for dam surface in early April 2016(Unit:MPa)



(a) 上游坝面



(b) 下游坝面

图10 4月上旬坝面最小主应力分布(单位:MPa)

Fig. 10 Minimum principal stress distribution for dam surface in early April 2016(Unit:MPa)

4.3 应力仿真计算结果

基于反演得到的温度场与材料弹性模量,仿真得到2016—2018年小湾拱坝应力分布。

限于篇幅只展示2016年4月上旬与10月上旬坝面应力分布情况(图9~14),其中拉应力为正、压应力为负,从图中可以看出:上游坝面基本处于受压状态,其最大压应力在10 MPa左右,位于上游坝面975 m高程处;在1—5月,由于温度较低,上游坝面水位以上部分出现拉应力区,最大拉应力在0.6 MPa左右;下游坝面水位以下部分,基本呈现出受压状态,最大压应力可达17.3 MPa,位于下游坝面坝趾处;下游坝面大部分区域处于受压状态,在坝基交界面附近由于应力集中出现局部拉应力,全局最大拉应力在0.8 MPa左右,但不至于影响工程安全运行。

表4 材料弹性模量反演结果

Tab. 4 Elastic modulus inversion results of materials

单位:GPa

混凝土分区				基岩类别						
A	B	C _R	C _L	I _R	I _L	II a	II b	II c	II d	III
40.20	40.50	38.50	40.90	30.00	35.00	27.00	25.00	25.00	23.00	10.00

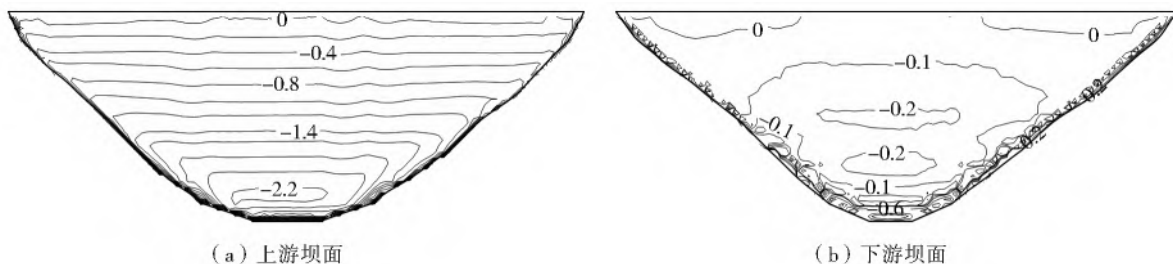


图 11 10 月上旬坝面最大主应力分布(单位:MPa)

Fig. 11 Maximum principal stress distribution for dam surface in early October 2016(Unit:MPa)

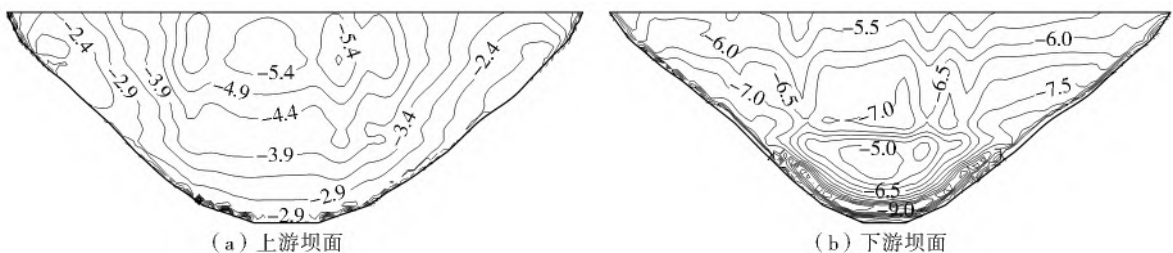


图 12 10 月上旬坝面最小主应力分布(单位:MPa)

Fig. 12 Minimum principal stress distribution for dam surface in early October 2016(Unit:MPa)

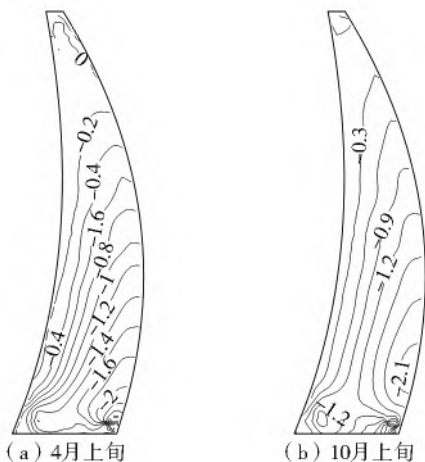


图 13 2016 年拱冠梁断面最大主应力分布(单位:MPa)

Fig. 13 Maximum principal stress distribution of crown beam section in 2016(Unit:MPa)

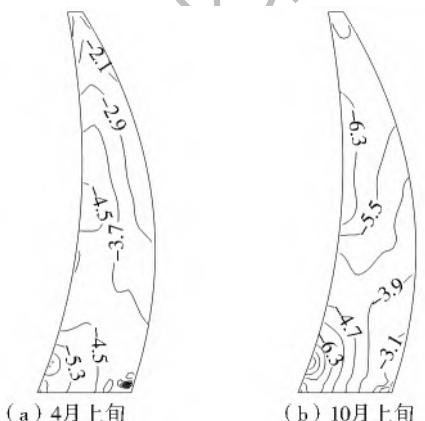


图 14 2016 年拱冠梁断面最小主应力分布(单位:MPa)

Fig. 14 Minimum principal stress distribution of crown beam section in 2016 (Unit:MPa)

5 结 论

本文采用有限元方法,基于小湾拱坝原型观测

资料,反演分析了其运行期全坝段温度场、坝体与基岩的弹性模量;根据反演结果,进行了小湾拱坝运行期应力仿真分析。得出以下结论:

(1)小湾拱坝下游坝面温度受气温影响较大,呈现两侧坝段温度较高、中间坝段温度较低的规律。

(2)小湾拱坝运行期间材料的弹性模量相对于试验值有一定提高,提高约 30%。

(3)小湾拱坝上游坝面在运行期基本处于受压状态,在 1—5 月,由于温度较低,可能在水位以上坝面出现一定的拉应力区域;运行期下游坝面最大压应力可达 17.3 MPa,位于下游坝面坝趾处,在坝基交界面附近由于应力集中出现局部拉应力区域,但并不至于影响工程安全运行。

参考文献(References):

[1] 朱伯芳. 大体积混凝土温度应力与温度控制[M]. 北京:中国水利水电出版社,2012. (ZHU B F. Thermal stresses and temperature control of mass concrete[M]. Beijing, China Water & Power Press,2012. (in Chinese))

[2] 袁琼. 二滩拱坝温度场及温度作用反馈分析[J]. 水电站设计,2003,19(1):20-25. (YUAN Q. Feedback analysis of Ertan arch dam temperature field and temperature effect[J]. Design of Hydroelectric Power Station, 2003,19(1): 20-25. (in Chinese)) DOI: 10. 3969/j. issn. 1003-9805. 2003. 01. 005.

[3] ORLOB G T., SELNA L G. Temperature variations in deep reservoirs[J]. ASCE Journal of the Hydraulics Division,1970,96(2): 391-410. DOI: 10. 1061/jyceaj. 0002337.

[4] GAL G, IMBERGER J, ZOHARY T, et al. Simulating

- the thermal dynamics of Lake Kinneret. *Ecological Modelling*, 2003, 162 (1/2): 69-86. DOI: 10. 1016/S0304-3800(02)00380-0.
- [5] 王进廷,王吉焕,刘毅,等.二滩拱坝运行期坝体温度场反馈分析[J].水力发电学报,2008,27(2):65-70. (WANG J T,WANG J H,LIU Y,et al. Feedback analysis on temperature field of Ertan arch dam in operation period[J]. *Journal of Hydroelectric Engineering*, 2008,27(2):65-70. (in Chinese)) DOI: 10. 3969/j. issn. 1003-1243. 2008. 02. 013.
- [6] JIN F,CHEN Z,WANG J T,et al. Practical procedure for predicting non-uniform temperature on the exposed face of arch dams[J]. *Applied Thermal Engineering*, 2010,30(14/15):2145-2156. DOI:10. 1016/j. applthermaleng. 2010. 05. 027.
- [7] 杨剑,王进廷,王吉焕,等.二滩拱坝及坝基材料参数反馈分析[J].水力发电学报,2008,27(2):78-83. (YANG J,WANG J T,WANG J H,et al. Feedback analysis of material parameters of ertan arch dam and its foundation rock[J]. *Journal of Hydroelectric Engineering*, 2008,27(2):78-83. (in Chinese)) DOI: 10. 3969/j. issn. 1003-1243. 2008. 02. 015.
- [8] 王平,朱维申,王可钧,等.单纯形法及其在广蓄电站围岩变形反分析中的应用[J].岩土学报,1991,12(2):57-65. (WANG P,ZHU W S,WANG K J,et al. Simplex acceleration method and its application to back analysis of measured displacement in surrounding rocks of GPSH[J]. *Rock and Soil Mechanics*, 1991,12(2):57-65. (in Chinese)) DOI: 10. 16285/j. rsm. 1991. 02. 009.
- [9] 李守巨,刘迎曦,王登刚,等.岩石和混凝土材料参数识别的修正高斯-牛顿算法[J].岩土力学与工程学报,2000,19(1):93-96. (LI S J,LIU Y X,WANG D G,et al. Material parameters identification of rock and concrete with modified GAUSS-NEWTON algorithm [J]. *Chinese Journal of Rock Mechanics and Engineering*, 2000,19(1):93-96. (in Chinese)) DOI:10. 3321/j. issn:1000-6915. 2000. 01. 021.
- [10] ARDITO R,BARTALOTTA P,CERIANI L,et al. Diagnostic inverse analysis of concrete dams with static excitation[J]. *Journal of the mechanical behavior of materials*, 2004, 15 (6): 381-389. DOI: 10. 1515/JMBM. 2004. 15. 6. 381.
- [11] 方卫华,徐兰玉,乐国兴,等.改进粒子群算法在大坝力学参数分区反演中的应用[J].大坝与安全,2012,30(5):30-34. (FANG W H,XU L Y,LE G X,et al. Investigation on divisional of dam mechanic parameters based on improved PSO algorithms[J]. *Dam and Safety*, 2012, 30 (5): 30-34. (in Chinese)) DOI: 10. 3969/j. issn. 1671-1092. 2012. 03. 008.
- [12] 王朝辉,贾宇峰,迟世春.基于粒子群算法的鲤鱼潭大坝坝料动参数反演[J].人民长江,2016,47(19):96-101. (WANG Z H,JIA Y F,CHI S C. Dynamic material parameter inversion of Liyutan earth dam based on particle swarm optimization[J]. *Yangtze River*, 2016,47(19):96-101. (in Chinese)) DOI: 10. 16232/j. cnki. 1001-4179. 2016. 19. 019.
- [13] 王峰,周宜红,赵春菊,等.基于改进粒子群算法的混凝土坝热学参数反演研究[J].振动与冲击,2019,38(12):168-174,181. (WANG F,ZHOU Y H,ZHAO C J,et al. Inverse analysis of concrete dam thermal parameters based on an improved particle swarm optimization method[J]. *Journal of Vibration and Shock*, 2019,38(12):168-174,181. (in Chinese)) DOI: 10. 13465/j. cnki. jvs. 2019. 12. 024.
- [14] 李端有,甘孝清,周武.基于均匀设计及遗传神经网络的大坝力学参数反分析方法[J].岩土工程学报,2007,29(1):125-130. (LI D Y,GAN X Q,ZHOU W. Back analysis on mechanical parameters of dams based on uniform design and genetic neural network[J]. *Chinese Journal of Geotechnical Engineering*, 2007,29(1):125-130. (in Chinese)) DOI: 10. 3321/j. issn: 1000-4548. 2007. 01. 022.
- [15] 俞祥荣,张社荣,王雪红,等.基于果蝇-BP神经网络算法的大坝力学参数反演[J].水利水电技术,2014,45(9):52-54. (YU X R,ZHANG S R,WANG X H,et al. Back analysis on dam mechanical parameters based on fruit fly-BP neural network algorithm[J]. *Water Resources and Hydropower Engineering*, 2014, 45(9): 52-54. (in Chinese)) DOI: 10. 3969/j. issn. 1000-0860. 2014. 09. 013.
- [16] 练继建,王春涛,赵寿昌.基于BP神经网络的李家峡拱坝材料参数反演[J].水力发电学报,2004,23(2):44-48. (LIAN J J,WANG C T,ZHAO S C. The convolute analysis of Lijiaxia arch dam material parameter based on BP neural network[J]. *Journal of Hydroelectric Engineering*, 2004, 23 (2): 44-48. (in Chinese)) DOI: 10. 3969/j. issn. 1003-1243. 2004. 02. 010.
- [17] 孙辅庭,张秀丽,王玉洁,等.基于改进遗传算法的大坝参数快速反演工具研究及应用[J].水力发电,2018,44(1):55-58. (SUN F T,ZHANG X L,WANG Y J,et al. Research and application of quick dam parameter inversion instrument based on improved GA [J]. *Water Power*, 2018, 44(1): 55-58. (in Chinese)) DOI: 10. 3969/j. issn. 0559-9342. 2018. 01. 014.
- [18] 邓祥辉,柴军瑞.自适应遗传算法在某拱坝渗流参数反演中的应用[J].西安石油大学学报(自然科学版),

- 2007, 22(2): 133-135. (DENG X H, CHAI J R. Application of adaptive genetic algorithm in the inversion of the seepage parameter of arch dam [J]. Journal of Xi'an Shiyou University (Natural Science Edition), 2007, 22(2): 133-135. (in Chinese)) DOI: 10. 3969/j. issn. 1673-064X. 2007. 02. 036.
- [19] 陈樊建, 朱岳明. 遗传算法在拱坝热学参数反演分析中的应用[J]. 华北水利水电学院学报, 2007, 28(2): 33-35. (CHEN F J, ZHU Y M. Application of genetic algorithms to the back analysis of thermal parameters in arch dam [J]. Journal of North China Institute of Water Conservancy and Hydroelectric Power, 2007, 28(2): 33-35. (in Chinese)) DOI: 10. 3969/j. issn. 1002-5634. 2007. 02. 010.
- [20] 马春辉, 杨杰, 程琳, 等. 基于量子遗传算法与多输出混合核相关向量机的堆石坝材料参数自适应反演研究[J]. 岩土力学, 2019, 40(6): 2397-2406. (MA C H, YANG J, CHENG L, et al. Adaptive inversion analysis of material parameters of rock 4-fill dam based on QGA-MMRVM [J]. Rock and Soil Mechanocs, 2019, 40(6): 2397-2406. (in Chinese)) DOI: 10. 16285/j. rsm. 2018. 0320.
- [21] 王勛成. 有限单元法 [M]. 北京: 清华大学出版社, 2003. (WANG X C. Finite element method [M]. Beijing: Tsinghua University Press, 2003. (in Chinese))
- [22] 苏怀智, 李季, 吴中如. 大坝及岩基物理力学参数优化反演分析研究 [J]. 水利学报, 2007 (S1): 129-134. (SU H Z, LI J, WU Z R. Feedback analysis for mechanical parameters of dam and its foundation with optimization algorithm [J]. Journal of Hydraulic Engineering, 2007(S1): 129-134. (in Chinese))
- [23] 韩世栋, 赵斌, 廖占勇, 等. 小湾特高拱坝蓄水初期垂线监测成果分析评价 [J]. 大坝与安全, 2010 (3): 38-41. (HAN S D, ZHAO B, LIAO Z Y, et al. Analysis and evaluation of monitoring data by plumb lines in early impoundment period of Xiaowan arch dam [J]. Dam and Safety, 2010 (3): 38-41. (in Chinese)) DOI: 10. 3969/j. issn. 1671-1092. 2010. 03. 012.

Feedback analysis on temperature field and stress simulation of Xiaowan arch dam in the operation period

ZHANG Mengzhong¹, PAN Jianwen¹, WANG Jinting¹, CHI Fudong²

(1. State Key Laboratory of Hydrosience and Engineering, Tsinghua University, Beijing 100084, China;

2. Huaneng Lancangjiang Hydroelectric Corporation Limited, Kunming 650214, China)

Abstract: The arch dam is a three-dimensional shell structure with a complex operating environment and complicated stress state, its actual working behavior is different from the design condition. During the operation of a high arch dam, the temperature load, which is determined by the difference between the temperature field during operation and its joint closure temperature field, is one of the main loads. Generally speaking, it is easy to obtain the temperature field of arch sealing. However, thermal analysis of the arch dam during operation is difficult due to the influence of climate conditions, structural form, and operation modes. In addition, as the main water-holding structure, the stress state of the arch dam during operation is sophisticated. The mechanical parameters of concrete may differ from the experimental values. Therefore, the research on the real working behavior of the Xiaowan arch dam is of great significance.

The material parameters of the Xiaowan arch dam were investigated and the stress distribution was simulated by the finite element method. The temperature distribution on the dam surfaces was fitted by the polynomial as the thermal boundary condition based on the measured temperature. Then transient temperature field of the Xiaowan arch dam was calculated step by step. The elastic modulus of dam concrete and foundation rocks were continuously adjusted to minimize the differentials between the numerical displacements calculated by FEM and the actual displacement measured by the plumb lines. The elastic modulus with the smallest displacement errors was viewed as the actual material parameters. The simulation of stress distribution of the Xiaowan arch dam was carried out based on the inversion results of the temperature field and material parameters.

Conclusions (1) The feedback temperature field could represent the temperature field distribution of the Xiaowan arch dam during the operation period. The temperature of the upstream dam surface was mainly affected by the reservoir water. Besides, the temperature of the upstream dam surface near the foundation was higher, between 17 °C and 19 °C due to the influence of the ground temperature and slag in front of the dam. The temperature of the downstream dam surface was mainly affected by atmospheric temperature, showing a phenomenon that the temperature was higher on both sides than in the middle section. (2) The elastic modulus of the dam concrete during the operation was increased by about 30% relative to the test value. Besides, the deformation modulus of the bedrock was 20%~45% higher than the test value. (3) The calculated displacement

(下转第 813 页)

ware. According to the results of numerical simulation, it is concluded that: (1) The velocity field in the mixing tank is axisymmetric concerning the submersible agitator. The flow is pushed forward along the center of the submersible agitator. When the central jet moves to the other side of the tank wall, the flow diffuses around. The area of velocity distribution cloud diagram in the mixing tank to achieve effective mixing becomes larger and larger with the increase of blade angle, which indicates that the mixing effect of submersible agitator becomes better and better when the blade angle increases from -4° to 4° . (2) The pressure distribution characteristics of the impeller pressure surface are almost the same under different blade placement angles, that is, the high-pressure area is mainly concentrated in the inlet area of the impeller, and the negative pressure area is concentrated in the area near the blade flange and impeller outlet. The pressure on the blade working surface increases with the increase of blade placement angle, that is, the area of the high-pressure area increases continuously. At the same time, the shaft power and thrust of the submersible agitator are increasing with the increase of blade angle. (3) Compared with the mixing effect, the effective mixing ratio and effective unit energy consumption of submersible agitators increase with the increase of blade angle. When the blade angle is -4° , the effective unit energy consumption of the submersible mixer is the minimum, and the effective mixing area in the mixing tank is only about half, and a part of low-speed zone or even dead zone will appear in the flow field, which affects the mixing effect. When the blade angle is increased to 4° , the mixing area of the submersible mixer is about 70% (the mixing effect of the submersible mixer has been improved in practical engineering application). Most of the fluid in the flow field has been stirred, which meets the design requirements, and the stirring effect is good. (4) Finally, to prove the accuracy of the numerical simulation results of submersible agitator, the experimental verification is carried out when the blade setting angle is 0° and the error between the numerical simulation and experimental verification is less than 5%, which proves the accuracy of the numerical simulation results. It shows that the research on the blade setting angle of the submersible agitator is feasible and provides a reference for the future research of submersible agitator certain reference.

Conclusions (1) With the increase of blade angle, the effective mixing area of velocity distribution nephogram in the mixing tank is increasingly larger, and the mixing performance of submersible agitator is improved. (2) When the blade angle increases from -4° to 4° , the shaft power and thrust of submersible agitator motor increase continuously. At the same time, with the increase of blade angle, the corresponding effective mixing ratio and effective unit energy consumption are also increasing. (3) The accuracy and rationality of the numerical simulation results are verified by experiments, which provides certain reference for the future research of submersible agitator.

Key words: submersible agitator; blade angle; numerical simulation; axial velocity

(上接第 794 页)

agreed well with the measured data with the same trend. The displacement of the Xiaowan arch dam was closely related to the upstream water level. The dam had a trend of slow deformation to the downstream because the aging effect had not yet fully converged at present. (4) The upstream dam surface was basically in a pressure state. Besides, the maximum compressive stress, which was located at the height of 975 m, was about 10 MPa. However, the dam surface above the water level was under tension in winter, and the maximum tensile stress was about 0.6 MPa. The downstream dam surface was basically in a compressive state, and the maximum compressive stress could reach to 17.3 MPa, which was located at the dam toe. Besides, the tensile stress zone appeared near the interface between the dam body and the foundation due to the stress concentration, and the global maximum tensile stress was about 0.8 MPa, although the operating state of the dam was still in the safe scope.

Conclusions (1) The temperature of the downstream dam surface was mainly affected by atmospheric temperature, showing a phenomenon that the temperature was higher on both sides than the middle section. (2) The elastic modulus of the dam concrete during the operation was increased by about 30% relative to the test value. (3) The stress distributions of the Xiaowan arch dam revealed that its operating state was still in the safe scope.

Key words: Xiaowan arch dam; temperature field; material parameters; inverse analysis; stress simulation